Catalysis Science & Technology

Accepted Manuscript

This is an *Accepted Manuscript*, which has been through the Royal Society of Chemistry peer review process and has been accepted for publication.

Accepted Manuscripts are published online shortly after acceptance, before technical editing, formatting and proof reading. Using this free service, authors can make their results available to the community, in citable form, before we publish the edited article. We will replace this *Accepted Manuscript* with the edited and formatted *Advance Article* as soon as it is available.

You can find more information about *Accepted Manuscripts* in the Information for Authors.

Please note that technical editing may introduce minor changes to the text and/or graphics, which may alter content. The journal's standard Terms & Conditions and the Ethical guidelines still apply. In no event shall the Royal Society of Chemistry be held responsible for any errors or omissions in this *Accepted Manuscript* or any consequences arising from the use of any information it contains.

ROYAL SOCIETY OF CHEMISTRY

www.rsc.org/catalysis

Catalysis Science & Technology

PAPER

Optimizing the dehydrogenation catalyst of higher normal paraffins supported on a nanocrystalline gamma alumina

Received 00th January 20xx,
Accepted 00th January 20xx

DOI: 10.1039/x0xx00000x
www.rsc.org/

Mandana Akia,[a]* Hamidreza Arandiyan,[b] Karen Lozano,[c] Seyed Mahdi Alavi [d]

This study presents an optimization of dehydrogenation catalysts components including platinum, indium, and lithium using response surface methodology (RSM). The catalysts were supported on a synthesized nanocrystalline gamma alumina and evaluated in the dehydrogentaion reaction of higher normal paraffins (C_{10}-C_{15}). The best catalytic performance was obtained with the following material ratios: 0.22 of Pt, 0.5 of In, and 0.31 of Li. Comparison the performance of the optimized catalyst to an industrial catalyst showed the improved catalytic activity of the optimized sample. The obtained results revealed the excellent potential of the optimized catalyst in higher normal paraffins undergoing a dehydrogenation reaction.

1- Introduction

Dehydrogenation catalysts of long chain paraffins are capable of being synthesized from a vast array of component mixtures (e.g., C_{10} to C_{13}, C_{11} to C_{14}, C_{11} to C_{15}).[1] The first successful catalytic dehydrogenation process goes back to 1935 when chromia-alumina catalysts were utilized in light hydrocarbon (e.g., n-C_2, C_3, C_4 and i-C_4) dehydrogenation process. In the 1960's, the usage of noble metal (e.g., Pt) catalysts for catalytic dehydrogenation was introduced with the intent to provide biodegradable detergent manufacturers with long chain linear olefins.[2,3,4] It has been proven that alumina supported Pt and Pt-containing bimetallic catalysts were employed in dehydrogenation process of heavy linear alkanes (C_{10}-C_{15}) and reforming naphtha in petrochemical plants.[5] Moreover, multimetallic catalysts supported on alumina, containing In and Sn promoters (i.e., platinum modifiers) along with alkaline and alkaline-earth metals (i.e., support modifiers) were implemented. [4,5,6] Studies on dehydrogenation catalysts for higher normal paraffins are rare and typically report the use of bimetallic catalysts. He et al. 2008, 2009 worked on the effect of carbon addition and also potassium addition on bimetallic (Pt-Sn) catalysts based on gamma alumina used in n-octadecane dehydrogenation reactions.[7] According to, Lai et al. 2015 studied the effect of a combined support Mg–Al–O for Pt–Sn catalysts in higher normal paraffins dehydrogenation reaction (normal dodecane as feedstock).[8] Li et al. modified the alumina support with Ce for Pt-Sn catalysts and used in the n-dodecane dehydrogenation reaction.[9] In the past several years, our group has extended attention to the synthesis and physicochemical property characterization of Pt-Sn catalysts. Akia et al. synthesized a nanostructured gamma alumina support and applied for the preparation of Pt-Sn catalysts containing indium, lithium and iron as modifiers.[10] In fact, the majority of the data concerning usage of multicomponent catalysts in higher normal paraffins dehydrogenation reaction has originated from granted patents.[11,12]

The activity and selectivity of olefins in the dehydrogenation reaction can be improved by the integration of Sn to the platinum catalyst while increasing the catalyst stability.[4,5] Alumina hydrogenating capacity is reduced when indium is used as a modifier while simultaneously suppressing cracking and isomerization of the olefins, the action is theorized to be result of the diminishing acidic functionality of the support. While the addition of Sn to Pt/Al_2O_3 catalysts has been investigated in several studies, the effect of Indium has not been fully exploited in dehydrogenation catalysts of higher paraffins.[13,14] The activity and stability of catalyst can also be increased via the integration of iron in the catalyst.[15] Due to its unparalleled capability in maintaining a high degree of platinum dispersion, which is necessary to achieve high dehydrogenation activity, alumina has become the standard support material in the development of dehydrogenation catalysts. However, the strongly acidic support can initiate side reactions (formation of diolefins and triolefins, aromatics and polymers) and the formation of coke.[1] Recently, this problem has been solved by the addition of alkaline and alkaline-earth ions (e.g., Li) to γ-Al_2O_3, which selectively poison active isomerization sites without harming the overall dehydrogenation capacity of the system.[6,16,17,18,19] Therefore, a novel strategy sol-gel technique first created by Yoldas, has been widely adopted for the production of highly porous

[a] Mechanical Engineering Department, University of Texas-Rio Grande Valley (UTRGV), Edinburg, TX 78539, USA. akia.mandana@gmail.com, mandana.akia@utrgv.edu
[b] Particles and Catalysis Research Group, School of Chemical Engineering, University of New South Wales, Sydney, NSW 2052, Australia. h.arandiyan@unsw.edu.au
[c] Mechanical Engineering Department, University of Texas-Rio Grande Valley (UTRGV), Edinburg, TX 78539, USA. karen.lozano@utrgv.edu
[d] Chemical Engineering Department, Iran University of Science and Technology, Tehran, Iran. alavi.m@iust.ac.ir

Catalysis Science & Technology Accepted Manuscript

Please do not adjust margins

alumina.[20] Response surface methodology (RSM) is a robust tool used in optimizing either the chemical reaction, preparation of the catalyst, or combination thereof and is known as a compilation of statistical methodologies employed when drafting experiments, creating models, defining variable relationships and determining optimum conditions. The benefits of RSM are as follows: provides a way to test how certain variables (e.g., process variables) affect the specified response; determines potential interrelationships among said variables; and characterizes the combined effects of variables in the resultant responses.[21] C. Bouchy et al. applied response surface method for alumina supported "Pt-Sn-X" in dehydrogenation of normal decane. Based on the results were reported for all the catalysts, design of experiments was confirmed as an important tool to maximize the catalyst selectivity.[19]

To the best of our knowledge, only a few reports on the successful dehydrogenation catalyst of higher normal paraffins have so far been seen in the literature. Herein, we report for the first time optimization of the dehydrogenation catalysts of higher normal paraffins supported on a nanostructured synthesized gamma alumina using the RSM method.

2- Experimental

2.1. Materials

The catalyst composite was composed of hexachloroplatinic acid (H_2PtCl_6), tin chloride ($SnCl_2$), iron nitrate ($Fe(NO_3)_3$), lithium nitrate ($LiNO_3$), indium chloride ($InCl_3$), and hydrochloric acid (HCl). Aluminium isopropoxide (AIP, 99 wt %), nitric acid, along with hexadecyl trimethylammonium bromide (C_{16}TMABr, 99 wt %) were used as support materials. All the materials were procured from Merck Co., except Hexachloroplatinic which was bought from the Riedel Company.

2.2. Support and catalyst preparation

The methodology employed in the preparation of the support was built upon already established procedures found in literature.[10,20] First, water was used to dissolve aluminum isopropoxide and hexadecyltrimethyl ammonium bromide. The molar ratio of water- to-AIP was 80:1 and the molar ratio of hexadecyltrimethyl ammonium bromide-to- AIP was 0.8:1. Hydrolysis was performed at 80°C, over 30 minutes while maintaining vigorous stirring. Afterwards, nitric acid (10 wt %) was utilized to peptize the mixture while being vigorously stirred via precise pH adjustment to achieve a pH value of 4.5. Aging of the mixture took place over 5 hours at ambient temperature. The mixture condensation was achieved via solvent evaporation, accomplished by raising the temperature of the reaction followed by a drying step in a 110 °C oven over 15 hours. This sample was then calcined (600 °C, 5 hours) to ensure surfactant removal, thus yielding the gamma crystallite phase.

The dehydrogenation catalyst is comprised of a synthesized gamma alumina support containing various weight percentages of Pt, Sn, In, Fe, and Li as well as < 0.1 wt% Cl. The wet impregnation method was used in the preparation of the catalyst which was consisted of three impregnation phases: phase one: Fe, Sn, and In; phase two: Pt; and phase three: Li. The co-impregnation of Sn, In, and Fe was carried via the incipient-wetness method on the gamma alumina support in a $SnCl_2$, In $(Cl)_3$, Fe $(NO_3)_3$, and 10 wt % HCl solution. We have carried out the catalytic performance with different ratio of iron and observed that addition of 0.2 wt% Fe would be beneficial for the enhancement in catalytic performance of the sample. After being well mixed by stirring, aging of the mixture is accomplished in ambient conditions after 4 hours. The mixture is then dried (vacuum oven at 80 °C, 18 hours) and calcined (540 °C, 2 hours in air atmosphere). Next, the incipient-wetness technique was also utilized to impregnate the dried sample with an aqueous solution (H_2PtCl_6, 10 wt % HCl) to attain the desired Pt content. The aging and drying steps were completed in the same manner as described in the initial phase. To mitigate side reactions, reduction of the Cl content (<0.1 wt %) was completed via wet calcination in a specific atmospheric mixture (50:50 molar ratio, air: water). The obtained samples were then further calcined (air atmosphere, 500 °C, and 2 hours). Finally, impregnation of the dehalogenated product, via an aqueous $LiNO_3/HNO_3$ solution, was completed through identical drying and calcination methods. An inductive coupled plasma (ICP) technique was then employed to analyze the final products. The results of inductive coupled plasma atomic emission spectroscopy (ICP–AES) investigation reveal that actual concentrations which were in agreement with theoretical estimate.

2.3. Characterization

All of the as-prepared samples were characterized by means of automated gas adsorption analyzer (Tristar 3000, Micromeritics) was employed to determine BET (Brunauer, Emmet, and Teller) surface area as well as the pore size distribution and volume via N_2 adsorption (-196° C). Transmission electron microscopy (TEM) (JEM-2100UHR, JOEL) was also completed at 200 KV. Preparation of samples for TEM analysis have been carried out by grinding, suspending and then sonicating of 5 mg of sample in ethanol. A drop of the prepared suspension was placed on a carbon-coated Cu grids, followed by ethanol evaporation. Scanning electron microscopy (SEM) (S-4800 FE-SEM, HITACHI) was performed at 5 kV. Determination of the true elemental contents within the catalysts was completed by ICP-AES (ICPV-1000, Shimadzu). Temperature programmed reduction (TPR) alongside temperature-programmed desorption of ammonia (NH_3-TPD) analyses were undertaken as well (ChemBET-3000 TPR/TPD Quantachrome plus thermal conductivity detector). For NH_3-TPD analysis, at first the sample was treated in a helium flow (30 mL min^{-1}) at 400˚C for 2 hours and then cooled down to 150˚C. In the next step, ammonia (30 mL min^{-1}) was introduced into the reactor for 40 minute. The unadsorbed gases were purged out of the reactor by helium flow and finally the sample was heated by increasing the temperature with a rate of 10˚C /min up to 700˚C. Temperature-programmed oxidation (TPO) profiles were obtained via a comparable apparatus through the introduction of a gas flow (30 mL min^{-1}; O_2: He, 5:95) over 50 mg of the used catalysts while increasing the thermal conditions to 800 °C at a specified ramp rate (10 °C /min).

2.4. Experimental design

Table 1 displays the three independent variables at three levels used for the Box-Behnken design. Three important variables, Platinum (X_1), Indium (X_2) and Lithium (X_3) contents, were considered for the optimization of dehydrogenation catalyst. Determination of the runs required for the Box- Behnken design was found by solving the following expression:

This journal is © The Royal Society of Chemistry 2015

Please do not adjust margins

Catalysis Science & Technology Accepted Manuscript

$$N = 2^k + 2k + m \quad \text{(Eq. 1)}$$

where N represents the total number of experimental runs, k stands for the number of considered parameters, and m refers to the number of replicates for the center point with one being the default value. The design was found to need 15 experiments, with three central point runs needed to evaluate the optimized method's reproducibility. Table 2 illustrates the independent variables' Box-Behnken method arrangement against their BET surface area. The obtained samples were respectively denoted as DH-1 to 15, in which the "DH" represents the use of Dehydrogenation catalyst.

Table 1. Box-Behnken design and independent variables for dehydrogenation catalysts optimization

Variables	Levels		
	Low	Medium	High
X_1	0.1	0.3	0.5
X_2	0.1	0.3	0.5
X_3	0.3	0.45	0.6

Table 2. Independent variables in Box-Behnken design along with their corresponding BET surface area

Run	X_1	X_2	X_3	Catalyst name	BET area ($m^2 g^{-1}$)	Pore diameter (nm)	Pore volume ($cm^3 g^{-1}$)
1	0.1	0.3	0.30	DH-1	203	7.7	0.39
2	0.5	0.5	0.45	DH-2	201	7.4	0.37
3	0.3	0.3	0.45	DH-3	206	7.6	0.39
4	0.1	0.5	0.45	DH-4	227	7.5	0.45
5	0.3	0.3	0.45	DH-5	203	7.6	0.40
6	0.3	0.3	0.45	DH-6	204	7.6	0.38
7	0.1	0.1	0.45	DH-7	227	7.8	0.48
8	0.3	0.5	0.60	DH-8	226	7.3	0.46
9	0.3	0.1	0.60	DH-9	226	7.8	0.46
10	0.1	0.3	0.60	DH-10	234	7.3	0.50
11	0.5	0.3	0.30	DH-11	233	7.8	0.53
12	0.5	0.3	0.60	DH-12	214	7.6	0.46
13	0.3	0.1	0.30	DH-13	218	7.9	0.44
14	0.5	0.1	0.45	DH-14	226	7.4	0.37
15	0.3	0.5	0.30	DH-15	214	7.6	0.41

2.5. Experimental setup for catalyst evaluation

The evaluation of the catalysts included the following significant experimental arrangements: section for hydrogen flow; a system for pumping the liquid feedstock; preheating and mixing section; reactor; condenser and separator for gas–liquid; and sufficient flow meters for the material balance. The reactor was comprised of the following attributes: fixed-bed quartz tubular microreactor (i.d=8 mm), isothermally operated, down-flow mode active, internal temperature monitoring via a central temperature probe (3 thermocouples), and inlet pressure monitored via pressure transmitter. The operating conditions are as follows: temperature (460-490 °C), pressure (1.7 bar); liquid hourly space velocity (LHSV) of feed: 20 h^{-1}; and hydrogen/hydrocarbon molar ratio: 6:1. The reaction utilizes hydrogen in such a way to ensure hydrogen to hydrocarbon molar ratio of approximately 6:1 due to the dehydrogenation of lower and higher paraffins requires hydrogen to be in excess. Hydrogen not only dilutes the paraffin but also suppresses hydrogen deficient, carbonaceous deposit formation on the catalyst composite. [4,12] The feedstock composition are presented in Table 3.

Table 3. The feed composition (wt%) for the dehydrogenation reaction

Component	wt %
N-C9	0.15
N-C10	7.16
N-C11	25.78
N-C12	29.46
N-C13	24.05
N-C14	7.18
N-C15	2.67
N-C16+	0.757
Total non normal (T.N.N)	2.793

3. Results and discussion

3.1. Texture and surface properties of catalysts

Shown in Figure 1 are the representative N_2 adsorption–desorption isotherms and pore-size distributions of the DH-3, DH-4 and DH-7 samples, and their pore parameters and surface areas are summarized in Table 2. The standard type IV nitrogen adsorption–desorption isotherm, according to IUPAC classification,[22] can be seen in Figure 1(a) along with typical mesoporous solids' H1 hysteresis loop in the relative pressure (p / p_0 = 0.7–0.9) which is suggestive of a broad distribution of pore diameters that consist of a uniform size and shape.[8] Pore size not only play an important role on the specific surface area,[2] but also it is significant for controlling diffusional resistance.[1] The diffusion rate of olefins out of pores is very important as the longer residence times lead to a decrease in selectivity and consequently increase the deactivation of the catalyst.[23] Figure 1 (b) displays the pore size distributions for the above mentioned samples. This graph displays that all of the samples show broad pore size distributions. The results of other catalysts also reflected mesostructured catalysts with wide pore size distributions.

3.2. Temperature programmed reduction (TPR)

Reducibility of a material is highly related to its catalytic performance. Figure 2 illustrated the H_2-TPR profiles of the DH-2, DH-9 and DH-12 samples. As it can be seen, there were two distinct reduction peaks were observed in all samples within a temperature range of 300-550 °C; these peaks also appeared in the other prepared samples. The first peak corresponds to the reduction of dispersed oxychloride species (PtClxOy) strongly interacting with the alumina support. The second peak is related to the reduction of other oxides (promoters) which presents a lower reduction temperature in comparison to the oxides alone, indicating the reduction of oxides has been facilitated by platinum atoms.[2]

Catalysis Science & Technology Accepted Manuscript

Please do not adjust margins

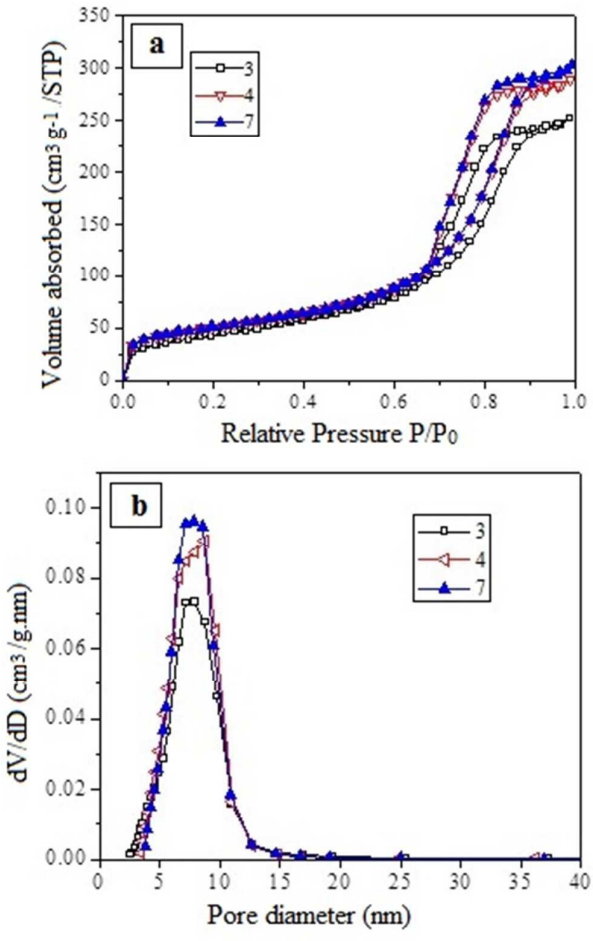

Figure 1. Nitrogen adsorption/desorption isotherms (a) and pore size distributions of DH-3, DH-4 and DH-7 catalysts (b)

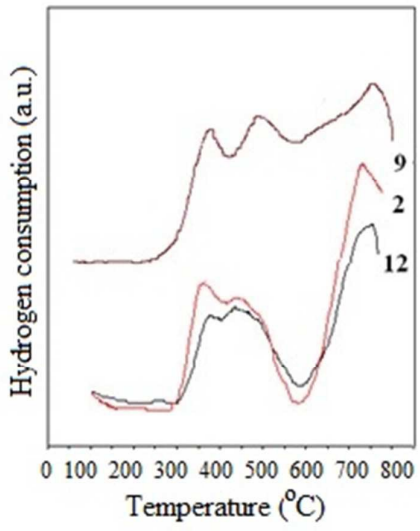

Figure 2. The TPR profiles of samples DH-2, DH-9 and DH-12

3.3. *Scanning electron microscopy (SEM) and Transmission electron microscopy (TEM)*

Figure 3(a, b) shows the SEM images of the DH-13 and DH-14 samples. These images indicate that the surfaces are not even and the void area can be attributed to the high surface area of the synthesized samples. It is known that the nano crystalline gamma alumina can support the conversion of the metal precursor(s) to a solid-state porous framework at 600 °C (5 hours) temperatures to access the high surface area and relatively large pore volume which could lead to excellent performance of the catalyst. As it can be seen in Figure 3(c), the observable darker areas are theorized to be clusters of metal whereas the lighter areas indicate the location of the nanocrystalline gamma alumina support. The spherical metal nanoparticles (NPs) deposited on the surface of gamma alumina plates were clearly observed in the range of nanometer in the TEM images. TEM results show a narrow metallic NPs distribution with a mean catalyst particle size of 2.6 (nm) which estimated by statistical analysis of more than 100 NPs. Pt NPs can be seen for DH-11 sample in the high resolution micrograph where the mean 2.2 nm of Pt NPs was dispersed on the nanocrystalline gamma alumina support which all of the Pt NPs were highly dispersed and uniform in size without any agglomerations, as indicated in Figure 3(d).

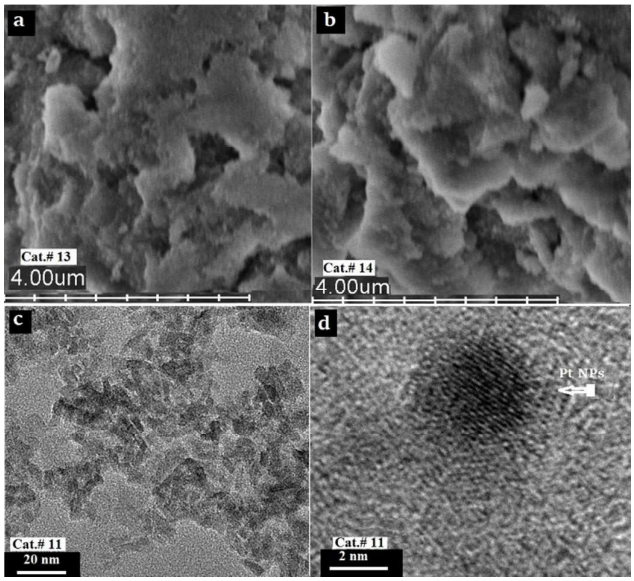

Figure 3. Scanning electron micrographs of DH-13 and DH-14 catalysts (a, b) and Transmission electron micrographs of DH-11 catalyst (c, d)

4. Catalytic performance

Table 4 summarizes the catalytic experimental data. Before undergoing evaluation, all samples were passed through a 20-40 mesh sieve and were activated under 10 vol% H_2/Ar (30 mL min^{-1}) whilst being heated to 430 °C (5 °C /min ramp) at which it was held for 4 hours. Testing was then completed over 18 hours period. The three temperatures used to carry out the dehydrogenation reactions were 460, 475, and 490 °C. Prior to entering the separator, a water cooler was used to reduce the temperature of the reactor effluent. The following components were analyzed via liquid analysis (FID detector, HP PONA column) on the final product: paraffins, olefins and diolefins, iso-paraffins, alkyl aromatics and alkyl naphthenes as well as cracked products. The results

Catalysis Science & Technology Accepted Manuscript

This journal is © The Royal Society of Chemistry 2015

Please do not adjust margins

determined that no diolefins were present. The catalytic activities increased with the rise in temperature while decreased in selectivity for all the samples, as shown in Table 4. The results confirmed the low decreasing variation of selectivity for all the samples with increasing the temperature.

5. Optimization results

5.1. Optimization of total conversion

Predicting the variable's effects was accomplished by employing the following quadratic model to evaluate the total conversion:

$$Y = b_0 + b_1X_1 + b_2X_2 + b_3X_3 + b_{12}X_1X_2 + b_{13}X_1X_3 + b_{23}X_2X_3 + b_{11}X_1^2 + b_{22}X_2^2 + b_{33}X_3^2 \quad \text{(Eq. 2)}$$

where Y is the measured response related to each parameter level combination; b_0 is an intercept; b_1 to b_{33} stand for the regression coefficients; and X_1, X_2, and X_3 represent the independent variables. As it can be seen in Table 5, the experimental data was fit to the total conversion resulting in the quadratic coefficients of equation. The P values, as shown in Table 5, were used to establish the coefficient's significance, where smaller P value imparted great significance to that particular model parameter. The determination coefficient (R^2) value of 98.2 indicates that the model accounted for most of the observed variation. The high adjusted determination coefficient results (Adj R^2 = 95) further confirms the model's significance.

The equation that follows is the result of adjusting the response variables for the quadratic model:

$$Y_1 = 6.66 + 9.54\times X_1 + 4.79\times X_2 + 9.95\times X_3 - 20.81\times X_1^2 - 9.31\times X_2^2 - 13.89\times X_3^2 + 3\times X_1X_2 - 2\times X_1X_3 + 5.83\times X_2X_3 \quad \text{(Eq. 3)}$$

where Y_1 is the total conversion. To be included in the model, coefficients had to make a significant contribution thus allowing it to be used as an accurate predictor. The total conversion as a function of Pt and In weight percentages is displayed as a surface plot in Figure 4(a) while the Li content is kept at the minimum value. With an increase in the Pt content in the region 0.1 - 0.25 wt %, the variation of total conversion is shown to be almost smooth. The lowest total conversion was obtained at the highest Pt content while the In content was held at its minimum value. Similar results were obtained for other values of Li content.

Table 4. The catalytic performances of the prepared samples at three different temperatures in higher normal paraffins dehydrogenation reaction

Catalyst	Temp. (°C)	Total Conversion, (%)	Monoolefins, (%)	Selectivity, (%)
DH-1	460	10.29	9.51	92.39
	475	12.73	11.42	89.70
	490	16.29	13.79	84.64
DH-2	460	9.73	8.57	88.09
	475	12.13	10.24	84.42
	490	16.35	13.33	81.53
DH-3	460	10.70	9.10	85.10
	475	14.55	12.29	84.42
	490	18.06	14.70	81.36
DH-4	460	10.62	9.18	86.49
	475	14.22	11.85	83.33
	490	17.06	14.13	82.83
DH-5	460	10.70	9.10	85.10
	475	14.55	12.29	84.42
	490	18.06	14.70	81.36
DH-6	460	10.70	9.12	85.21
	475	14.55	12.29	84.42
	470	18.06	14.70	81.36
DH-7	460	9.50	8.69	91.43
	475	11.82	10.04	84.94
	490	15.97	13.07	81.84
DH-8	460	10.36	9.25	89.29
	475	13.37	11.48	85.86
	490	16.66	13.33	80.04
DH-9	460	9.19	8.39	91.29
	475	12.79	10.91	85.33
	490	16.58	13.76	83.04
DH-10	460	10.05	8.98	89.37
	475	12.83	11.22	87.47
	490	17.74	15.31	86.30
DH-11	460	9.18	8.13	88.56
	475	12.20	10.43	85.53
	490	16.72	13.92	83.27
DH-12	460	8.70	7.86	90.41
	475	11.55	10.43	90.23
	490	15.46	13.89	89.87
DH-13	460	10.02	9.02	90.02
	475	13.68	12.07	88.25
	490	16.84	13.89	82.49
DH-14	460	8.13	7.35	90.08
	475	11.45	9.91	86.57
	490	14.76	12.17	82.46
DH-15	460	10.49	9.70	92.50
	475	13.35	12.14	91.01
	490	17.58	15.64	89.00

Catalysis Science & Technology Accepted Manuscript

Table 5. Testing the significance of regression coefficient of the quadratic model for total conversion response

Model term	Coefficient estimate	Standard error	P-value
Intercept	6.66	1.059	
X_1	9.54	2.061	0.006
X_2	4.79	2.061	0.068
X_3	9.95	3.931	0.052
X_1^2	-20.81	2.313	0.000
X_2^2	-9.31	2.314	0.010
X_3^2	-13.89	4.112	0.020
$X_1.X_2$	3.00	2.222	0.235
$X_1.X_3$	-2.00	2.963	0.106
$X_2.X_3$	5.83	2.953	0.0101

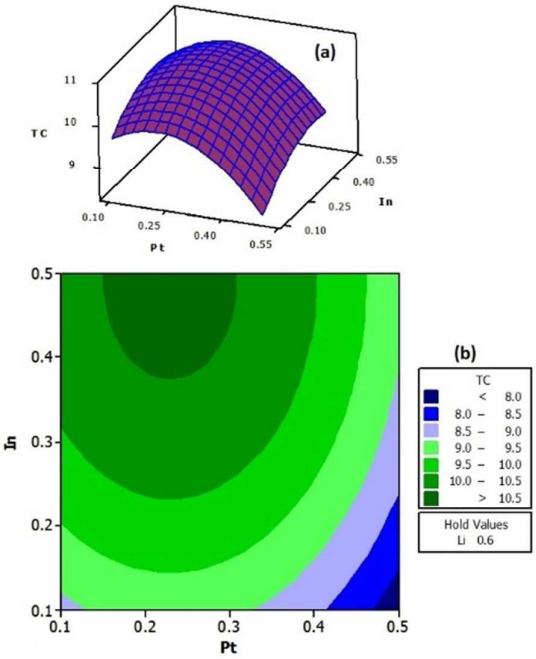

Figure 4. Response surface and contour plots of total conversion as a function of Pt and In contents, (a) at the minimum Li value, (b) at the highest Li content

The contour plot of Pt and In at the maximum Li content is shown in Figure 4(b). The results indicate that the maximum total conversion was obtained at the lower Pt contents and higher contents of In.

Figure 5(a) shows the variations of total conversion against Pt and Li contents while the content of In was held at its minimum value. The results revealed that when the Pt content was maintained between 0.2- 0.3 wt%, the maximum total conversion was obtained at different Li contents. The lowest value of total conversion was found at the highest Pt content value. Similarly, the effects were mirrored when In content was maintained at the medium and high values. Contour plot of Pt's and Li's effects at the maximum value of In content on the total conversion are displayed in Figure 5(b). The results clearly indicate that the best conditions to obtain the highest total conversion are 0.12 - 0.32 wt % for Pt and 0.32 - 0.55 wt % for Li content.

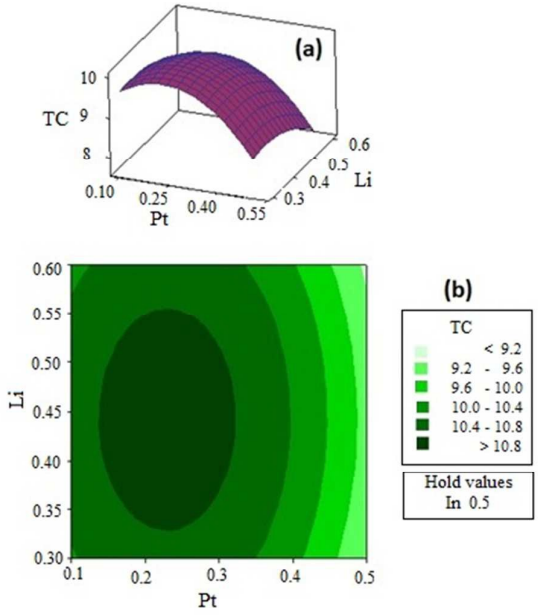

Figure 5. Response surface and contour plots of total conversion as a function of Platinum and Lithium contents: (a) at the minimum Indium value, (b) at the maximum Indium value

The total conversion at the highest Pt value as a function of In and Li contents is displayed as a surface plot in Figure 6(a). Increasing the In content at the lower values of Li resulted in slight increases in the total conversion. At higher values of Li, the total conversion significantly increases with increasing In content. Similar results were obtained for the other Pt contents. The contour plot of total conversion at the medium Pt content as a function of In and Li is presented in Figure 6(b). The highest total conversion was found to be at the conditions of In values higher than the medium content and Li content between 0.33-0.51 values.

5.2. Optimization of olefins selectivity

Full quadratic regression adjusted the optimization results for olefins' selectivity. The determination coefficient's value for olefins selectivity was 92.8% with the adjusted determination coefficient value being 79.8%. The P-values found in Table 6 were used to determine a coefficient's significance; lower P-values indicating a greater effect on the response. When the response variables were adjusted to the quadratic model, the following equation formed:

$$Y_2 = 128.6 - 48.8 \times X_1 - 26.2 \times X_2 - 137.6 \times X_3 + 42.1 \times X_1^2 + 58 \times X_2^2 + 151.2 \times X_3^2 + 17.9 \times X_1 X_2 + 37.3 \times X_1 X_3 - 40.6 \times X_2 X_3 \quad \text{(Eq. 4)}$$

where Y_2 is the olefins' selectivity response. It should be noted that the model incorporated those coefficients that made sizable contributions. As such, the resulting model may potentially serve as a functional predictor.

Catalysis Science & Technology Accepted Manuscript

This journal is © The Royal Society of Chemistry 2015

Please do not adjust margins

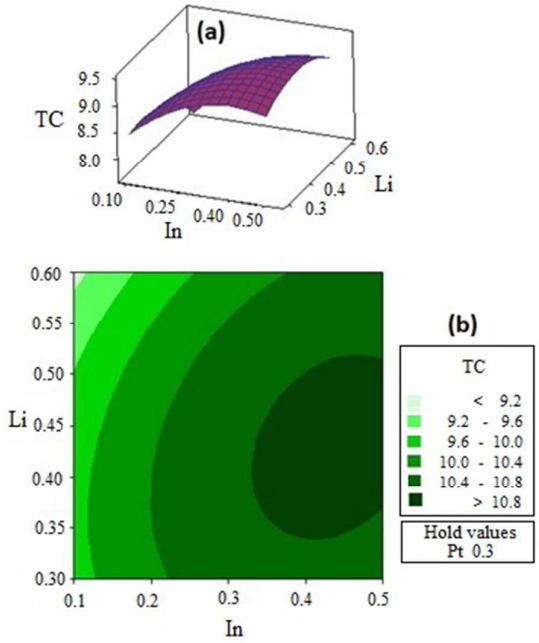

Figure 6. Response surface and contour plots of total conversion as a function of Indium and Lithium contents, (a) at the maximum Pt value, (b) at the medium value of Pt

Table 6. Significance test for regression coefficient of the quadratic model for olefins selectivity

Model term	Coefficient estimate	Standard error	P-value
Intercept	128.6	7.243	
X_1	-48.8	14.093	0.018
X_2	-26.2	14.093	0.122
X_3	-137.6	26.881	0.004
X_1^2	42.1	15.817	0.045
X_2^2	58	15.817	0.015
X_3^2	151.2	28.120	0.003
$X_1.X_2$	17.9	15.197	0.293
$X_1.X_3$	37.3	20.2 63	0.125
$X_2.X_3$	-40.6	20.253	0.102

The olefins' selectivity surface plot is expressed as a function of the contents of both Pt and In at the maximum value of Li content as displayed in Figure 7(a). According to the plot, with an increase in the Pt content to the medium value, selectivity slightly decreased and then it increased for the other Pt values. The minimum selectivity was obtained at the lowest values of Pt and higher value of In contents. Similar results were observed at the other values of Li content. The maximum selectivity was obtained at the lowest values of Pt and In contents. Figure 7(b) shows the effects of Pt and Li contents on the olefins' selectivity at the maximum value of In content. By increasing the Pt content over low to medium values of Li content, the olefins' selectivity initially shows a decrease to the medium Pt value and then increases. These variations indicated that in order to obtain the highest selectivity, the optimal conditions are at low content values of Pt and Li. The variation of selectivity was similar at the other values of In content as it is also seen in the contour plot shown in Figure 7(c). A selectivity plot is displayed in Figure 7(d) which is a function of In and Li contents at the highest Pt value. Increasing the Li content to a medium value caused a decrease in the selectivity and then selectivity increased with an increase in the Li content up to its maximum value. The decline rate is higher at the low values of In content compared to higher values. Maximum selectivity was obtained at the highest Li values and the lowest values of In content. The plots for other values of Pt content were similar to Figure 7(d).

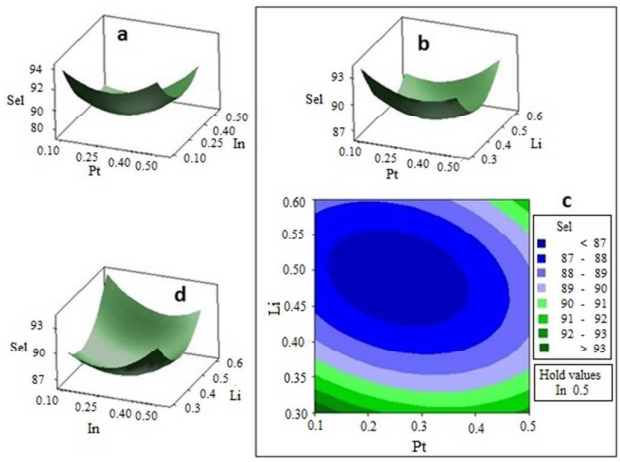

Figure 7. Olefins selectivity, (a) surface plot as a function of Pt and In at the maximum of Li content, (b, c) surface and contour plots as a function of Pt and Li at the maximum of In content and (d) surface plot as a function of In and Li at the maximum of Pt content

6. Conformity studies

The optimum conditions for obtaining the highest total conversion and selectivity as put forth in this study are 0.22, 0.5 and 0.31 for Pt, In and Li contents, respectively. The total calculated conversion and olefins' selectivity were 10.62 and 93%, respectively. The as-prepared sample yielded values of 10.4 and 92% for the total conversion and selectivity (at a temperature of 460°C), respectively.

6.1. Texture and surface properties of the optimized catalyst sample

The optimized N_2 adsorption–desorption isotherms of as-prepared sample showed the typical IV isotherm shape which is in accordance with the IUPAC classification, characteristic of mesoporous solids. The synthesized support's average pore diameter and pore volume along as well as BET surface area were 7.8 (nm), 0.51 (cm^3g^{-1}), and 232 (m^2g^{-1}), respectively.

6. 2. Catalytic activity

By employing a mixture of normal paraffinic feed (C_{10}-C_{15}), observation of the catalyst's behavior could take place. The resulting catalytic activity was also evaluated against DP-805 catalyst, an industrial IFP (Institut Francais du Petrole) catalyst used as a reference. The IFP catalyst composition is as follows: Pt 0.4 wt %; Sn 0.35 wt %; In 0.2 wt %; Li 0.35 wt %. Figure 8 presents the resulting catalytic behaviour of the optimized and industrial catalysts. Predictably, by raising the reaction temperature (460 °C to 490 °C), increases in total conversion were noted, however the

Catalysis Science & Technology Accepted Manuscript

Please do not adjust margins

olefins selectivity decreased. The results revealed that the total conversion and olefins selectivity were higher in the optimized catalyst when compared to the industrial sample (Figure 8(a)). In Figure 8(b), the catalytic results of the optimized sample (Op) and DP-805 (In) are presented after 48 hours on stream of reaction. A temperature of 460 °C was maintained along with all other test conditions apart from the H_2/HC molar ratio (1:1). Since hydrogen is used to limit coke formation while raising catalyst stability, its amount was decreased in order to determine the catalytic activity when subjected to severe circumstances.

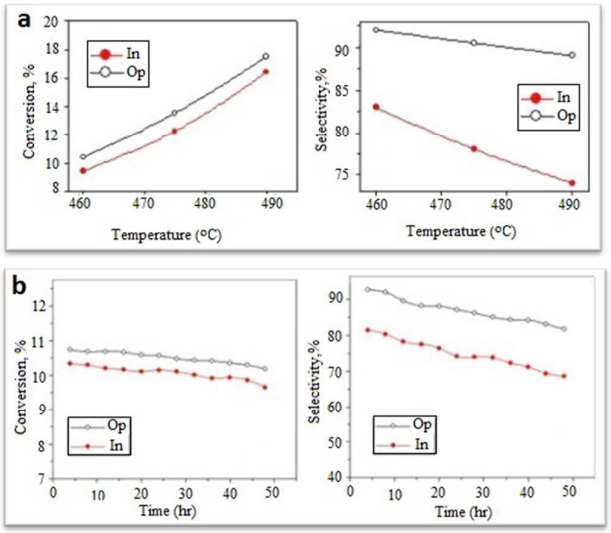

Figure 8. Conversion and selectivity for the optimized and industrial catalysts, (a) at three different temperatures and (b) at 460˚C for 48 hours on stream

The data gathered clearly reveals the optimized catalyst's increased mono-olefins' selectivity and conversion. The olefins selectivity of DP-805 sample reduced which might be due to the secondary dehydrogenation (i.e., diene conversion to an aromatic) along with parallel formation of light paraffins. The total conversion reductions were 4.21% and 6.25% in the optimized and industrial catalysts, respectively. In addition, the catalytic stability of the industrial and optimized samples were tested, in which reduction in mono-olefins selectivity were 11.8% for the industrial sample and 5.1% for the optimized sample after overall 48 hours test time. The rate of decrease in the olefins products were 1.34:1.00 in the industrial sample rather than the optimized catalyst. Such outcomes reflect the greater stability of the optimized catalyst when compared against the industrial catalyst. In addition, the Pt content in the optimized catalyst is almost half of that found in the industrial sample. This result is very promising due to the expense incurred from the Pt active phase.

6. 3. Temperature-programmed desorption of ammonia

Figure 9(a) shows the data obtained from the NH_3-TPD experiments using two samples (optimized and industrial catalyst). Using Narayanan's definition,[24] the desorbed ammonia values for the specified thermal ranges (i.e., 120 to 250 ℃, 250 to 350 ℃ and 350 to 450 ℃) were used to determine the acid sites' strength (i.e., weak, medium, and strong, respectively). As presented in Table 7, it can be concluded that almost all the acidic centers of the optimized catalyst are concluded to be weak to medium acid sites. If these sites are in excess, specifically those that are strongly acidic, induction of side reactions to form carbonaceous deposits (i.e., coke) will occur upon the movement of olefins to the acidic sites. As a result, the amount of side reactions occurring on the industrial catalyst is predicted to be greater than those in the optimized sample. Figure 9(b) shows the amount of diens and aromatics components which have formed after 48 hours of exposure to a dehydrogenation reaction. The results clearly confirmed the increase in the optimized catalytic stability when contrasted against the industrial catalyst sample.

Table 7. NH_3-TPD results and the acidic strength distributions of the optimized and industrial catalyst

Catalyst	T_{max}(˚C)			Acidity (mmol NH_3 g^{-1})	Peak fraction (%)		
	I	II	III		I	II	III
Op	141	232	556	6.45	0.62	0.26	0.12
In	148	230	580	10.19	0.18	0.38	0.44

6. 4. Temperature-programmed oxidation

Figure 9(c) illustrates that the carbon increased (i.e., coke formation) during the dehydrogenation reaction which lasted for 48 hours over the optimized and industrial samples. The peak at the lower temperature corresponds to the coke formation on the metal and the second peak at the higher temperature related to the coke located on the support.[25]

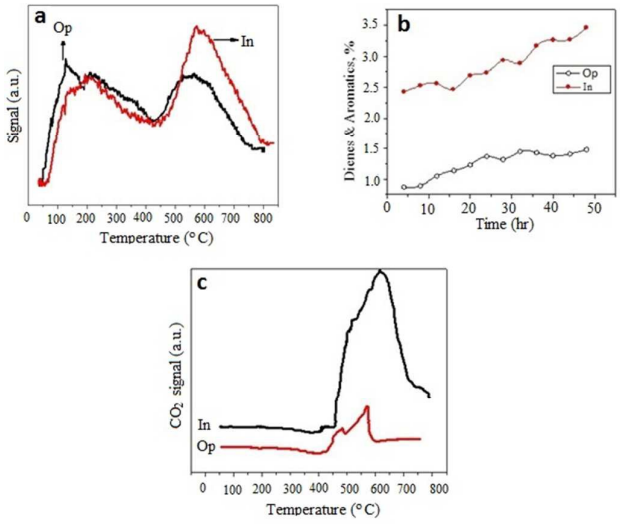

Figure 9. Comparison between the optimized (Op) and Industrial (In) catalysts properties, (a) NH_3-TPD profiles, (b) dienes and aromatics produced during 48 hours of dehydrogenation reaction and (c) TPO profiles for both catalysts

Comparison the maximum peak temperature for industrial and optimized catalysts clearly indicated the higher degree of graphitization for the industrial sample.[26] The total carbon deposited over the dehydrogenation catalyst is determined using the peak area of the TPO spectra. The amount of coke found on the industrial catalyst for the duration of the reaction period was approximately 7 times as much as that of found on the optimized catalyst. This is in agreement with the results obtained with the

Catalysis Science & Technology Accepted Manuscript

This journal is © The Royal Society of Chemistry 2015

Please do not adjust margins

previous studies which a key variable in determining catalyst deactivation for the dehydrogenation process is coke deposition.[1] Improvements in the optimized catalytic stability can be associated with the reduction in coke formation on the catalyst. The obtained results indicated more strong acidic sites in the industrial catalyst in comparison to that of the optimized sample, further confirming the TPD-NH_3 results.

7. Conclusions

Different dehydrogenation catalysts were prepared to study the effect of platinum as the active phase with indium and lithium as modifiers while using a synthesized nanocrystalline gamma alumina support. The optimized catalyst was identified by an optimization method. The optimized sample that was prepared at the optimum conditions showed efficient promising total conversion and selectivity in comparison to the industrial sample. The optimized catalyst showed a lower amount of side reactions versus that of the industrial sample, which is a consequence of the fewer strong acidic sites on the optimized catalyst. As dehydrogenation reaction is strongly endothermic, one method to achieve higher conversion is increasing the reaction temperature. However, increasing the side reactions and decreasing selectivity are inevitable in this condition. The results revealed that higher temperatures can be utilized to obtain higher yield using the optimized catalysts which can be mentioned as one of the advantages of the optimized catalyst. The amount of coke formation was almost seven times higher in the industrial catalyst sample when compared to the optimized catalyst. Generally, a lower rate of coke build-up is an advantage in dehydrogenation catalysts since the stability of catalyst increases. The optimized catalyst revealed very good stability during 48 hours of reaction time under severe conditions. The Pt content of the optimized catalyst was almost half of the amount measured in the industrial catalyst sample. As such, this study revealed that large quantities of platinum are not required due to the highly dispersed active phase found on the nanocrystalline gamma alumina support.

References

1 M.M. Bhasin, J. H. McCain, B. V. Vora, T. Imai, P. R. Pujadó, *Appl. Catal. A: Gen.*, 2001, **221**, 397.
2 S. He, C. Sun, Z. Bai, X. Dai, B. Wang, *Appl. Catal. A: Gen*., 2009, **356**, 88.
3 Y. Lai, S. He, X.Li, C. Sun, K. Seshan, *Appl. Catal. A: Gen*., 2014, **469**,74.
4 B.V. Vora, *Top Catal.*, 2012, **55**,1297.
5 D. Sanfilippo, I. Miracca, *Catal. Today*, 2006, **111**, 133.
6 J.A. Kent, Handbook of Industrial Chemistry and Biotechnology, 12 ed., Springer, New York, 2012.
7 S. He, C. Sun, H. Du, X. Dai, B. Wang, *Chem. Eng. J.*, 2008, **141**, 284.
8 Y. Lai, S. He, S. Luo, W. Bi, X. Li, C. Sun, K. Seshan, *Catal. Commun.*, 2015, **69**, 39.
9 X. Li, S. He, H. Wei, S. Luo, B. Gu, C. Sun, *J. Phys. Chem. A*, 2015, **89**, 1368.
10 M. Akia, S. Alavi, M. Rezaei, Z. F. Yan, *J. Porous Mater.*, 2010, **17**, 85.
11 A.G. Bozzano, S.W. Sohn, CA2857313A1, 2013.
12 G.J. Antos, US4366091 A, 1982.
13 A. Jahel, P. Avenier, S. Lacombe, J. Olivier-Fourcade, J. C. Jumas, *J. Catal.,* 2010, **272**, 275.
14 X. Liu, W. Z. Lang, L. L. Long, C. L. Hu, L. F. Chu, Y. J. Guo, *Chem. Eng. J.,* 2014, **247**, 183.
15 R.I.P.C.L. Dongara, K.K.I.P. Ramaswamy, US6635598 B2, 2001.
16 L.D. Sharma, M. Kumar, A.K. Saxena, M. Chand, J.K. Gupta, *J. Mol. Catal. A: Chem.*, 2002, **185**, 135.
17 C.L. Pieck, C.R. Vera, J.M. Parera, G.N. Gimenez, L.R. Serra, L.S. Carvalho, M.C. Rangel, *Catal. Today,* 2005, **107-108**, 637.
18 X. Li, S. He, H. Wei, S. Luo, B. Gu, C. Sun, *Chem. Kinet. Catal*., 2015, **89**, 1368.
19 C. Bouchy, P. Duchene, A. Faraj, *Oil. Gas. Sci. Technol*., 2013, **68**, 429.
20 M. Akia, S. Alavi, M. Rezaei, Z. F. Yan, *Microporous Mesoporous Mater.*, 2009, **122**, 72.
21 M.A. Bezerra, R.E. Santelli, E.P. Oliveira, L.S. Villar, L.A. Escaleira, *Talant*., 2008, **76**, 965.
22 M. Thommes, *Chem. Ing. Tech.*, 2010, **82**, 1059.
23 A.Lira, R.G. Tailleur, *Fuel*, 2012,**97**, 49.
24 S. Narayanan, A. Sultana, Q. Thinh Le, A. Auroux, *Appl. Catal. A: Gen.,* 1998, **168**, 373.
25 C.L. Pieck, P. Marecot, J.M. Parera, J. Barbier, *Appl. Catal. A: Gen.*, 1995, **126**, 153.
26 S. He, C. Sun, X. Yang, B. Wang, X. Dai, Z. Bai, *Chem. Eng. J.*, 2010, **163,** 389.

Catalysis Science & Technology Accepted Manuscript

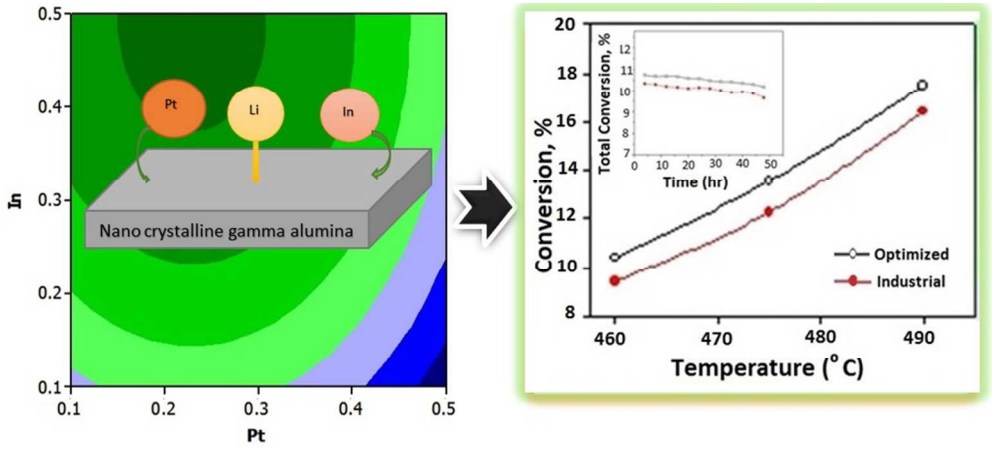

283x125mm (96 x 96 DPI)

Catalysis Science & Technology Accepted Manuscript